フィン付き流路内の流動・熱伝達特性に関する研究

5

Fluid Flow and Heat Transfer Analysis of Different Fin Patterns and Arrangement at a Narrow Duct.

5.1 Introduction

In this chapter we would like to investigate the fluid flow and heat transfer characteristics of finned surfaces of four different fin pattern, co-angular, zigzag, co-rotating and co-counter rotating pattern of different pitch ratio of 2, 3 and 3.5. Experiments were conducted for fins setting at a narrow duct of 50 mm height. Here we will discuss first the friction factor and the flow behavior of different fin pattern by smoke flow visualization and oil titanium oxide film flow visualization following a detailed discussion of the heat transfer characteristics. In addition we will compare the thermal performance of the fin patterns.

5.2 Flow visualization

5.2.1 Surface oil film flow patterns around fins at the endwall

The titanium oxide oil film flow patterns developed at the endwall for the co-angular, zigzag, co-rotating and co-counter rotating patterns are shown in Fig. 5.1(a) – (d). For the co-angular pattern as shown in Fig. 5.1 (a), for every fin row a horseshoe vortex was clearly observed in front of the fins. A separation line appeared at the first row from the mid position of the fins and then reattached at the back of the fins where vortex rolled up along the trailing edge of the fin. This type of vortex formation was also observed at lower Reynolds number by dye flow in water table around co-angular pattern in duct flow [2007]. A longitudinal vortex generated by the side top edge was also observed, which reattached to the inter fin region but could not touch the endwall shielded by the horseshoe vortex. The streak line in the figure also indicates that the

flow passed somewhat diagonally through the passage between the following fins. In that instance it was observed that flow contacted both side of the fins.

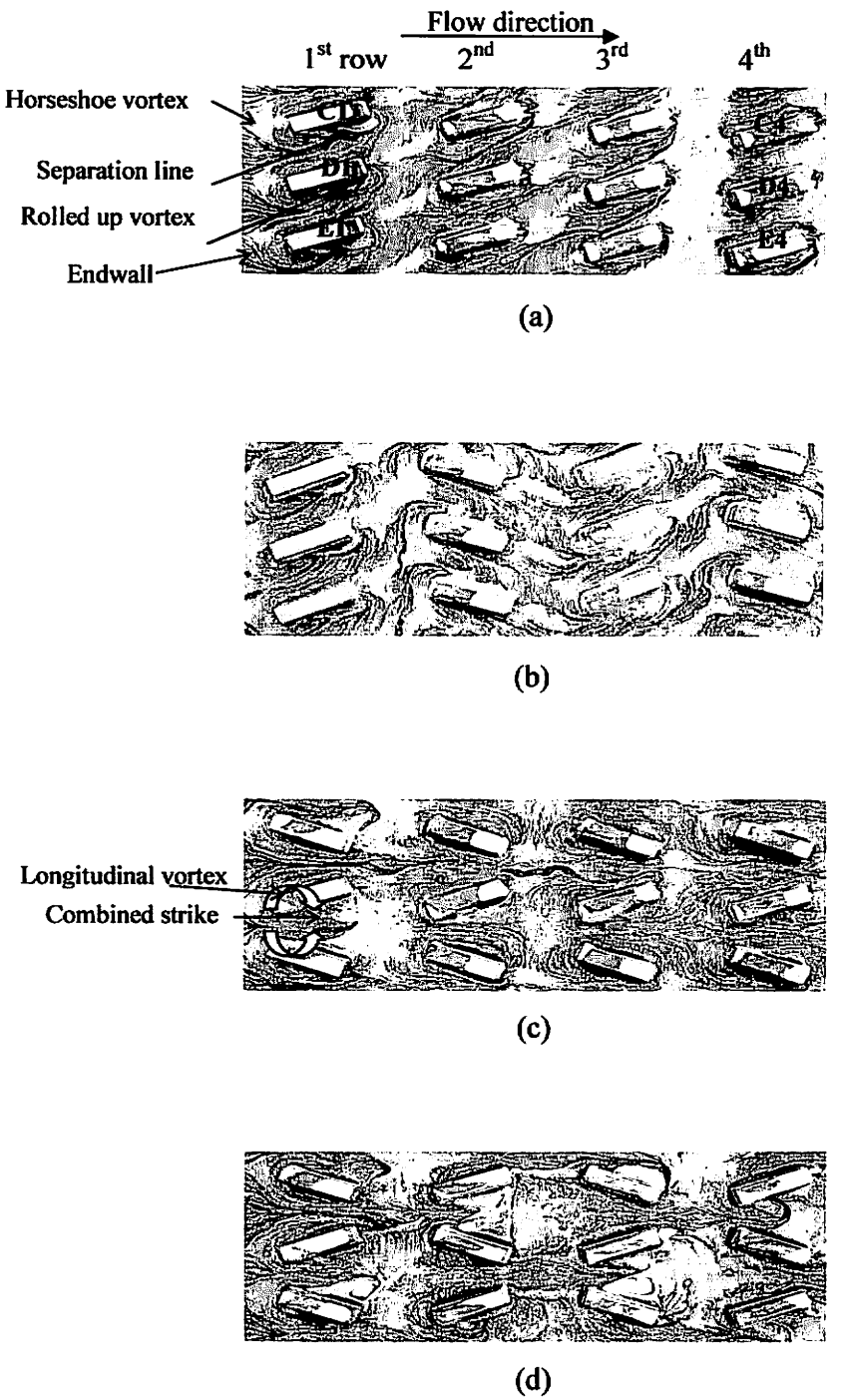

Fig.5.1 Titanium oxide oil film flow pattern at the endwall with (a) co-angular, (b) zigzag, (c) co-rotating and (d) co-counter rotating pattern for H_f=10 mm, Re = 10.44 × 10^4 in the duct flow.

The flow pattern at the endwall around the zigzag pattern is shown in Fig.5.1 (b) and it looks different than that of co-angular case as shown in Fig. 5.1 (a). Though a strong horseshoe vortex was clearly observed around the upstream side fins but the streak line appearance indicates that the strength of the vortex was decreased at downstream side fins. The longitudinal vortex generated by the side top edges touched the front side of the fins and the nearby endwall. The rear sides of the fins were lightly touched. As the directions of the fins alternated, flow could not pass diagonally, rather flowed in a sinusoidal wavy pattern.

Flow pattern in case of co-rotating pattern as shown in Fig.5.1 (c) looks different than that of previous cases though the horseshoe vortices are formed at the leading edge of every fin rows. As the converging pair forms a narrow exit at the trailing edge, flow velocity is increased which is clearly demonstrated by oil film flow. Streak line behavior indicates that flow reattached at the trailing edge and then form rolled up vortex as shown in Fig.5.1 (c) which enhance heat transfer in that region. Longitudinal vortex generated by side top edge of diverging fin pair was also observed which struck the endwall between the fin pair very strongly. Here, longitudinal vortexes were generated by both fins and combinedly struck the endwall which enhanced the heat transfer from that region. This flow effect will be further analyzed later with the thermal image. Streak line appearance is found similar for every fin rows.

In co-counter rotating pattern as shown in Fig. 5.1 (d), first row fins exhibit same oil flow pattern as that of co-rotating case. As the consecutive second fin rows are counter rotating (opposite rotation) type, the flow behavior of the second row shows different than the first fin row. Flow around third and fourth fin rows are similar to that of first and second fin rows respectively. Horseshoe vortices are not strongly observed.

5.2.2 Smoke flow visualization

The flow behavior and the flow pattern developed for the rectangular fin of co-angular, zigzag, co-rotating and co-counter rotating pattern are more clearly observed in smoke flow visualization as shown in Fig. 5.2 (a) – (d). In this visualization shadow of the fins are appeared and could not be completely removed as the fin ends were black painted to eliminate reflection. In case of co-angular pattern, at the leading edge (front) of the first row fins, horseshoe vortex was clearly observed and this vortex exists at the leading edge of every fin rows. At the trailing edge, behind the fin, rolled up vortex was also appeared due to low pressure at that region and this vortex was also observed at every fin rows. Flow reattached at the middle of front side face of the fins. Longitudinal vortex generated by the side top edge of the first row fins strike the endwall and continues to move and touch the inter fin region as well as the following fins.

In case of zigzag pattern horseshoe vortex same as that of co angular pattern was also observed at the leading edges of the first row fins. Horseshoe vortexes were not so clear at the leading edge of the second row fins. Vortex formed at the trailing edge of the first row fins combined with the incoming flow and then strongly hit the front side of the consecutive following fins as the zigzag pattern forms a sinusoidal wavy flow pattern. Flow got a good chance to wash the inter fin region and the leading edge of the second row fins though back side of the second row fins were not strongly touched. Flow behavior around co-angular and zigzag pattern has the similarity with that of dye flow in water table [2007]. Flow behavior around the co-rotating pattern is looked different than that of the previous cases. Longitudinal vortex generated by the diverging pair of first row fins combined and then struck the endwall between the pair and continues moving further downstream. In this instance it should be mentioned that the consecutive pair of the second row fins formed the same vortex and joined with the previous one. At the trailing exit of the converging fin pair, flow velocity was increased and stronger rolled up vortices were appeared at the middle position between the first and second row fins that

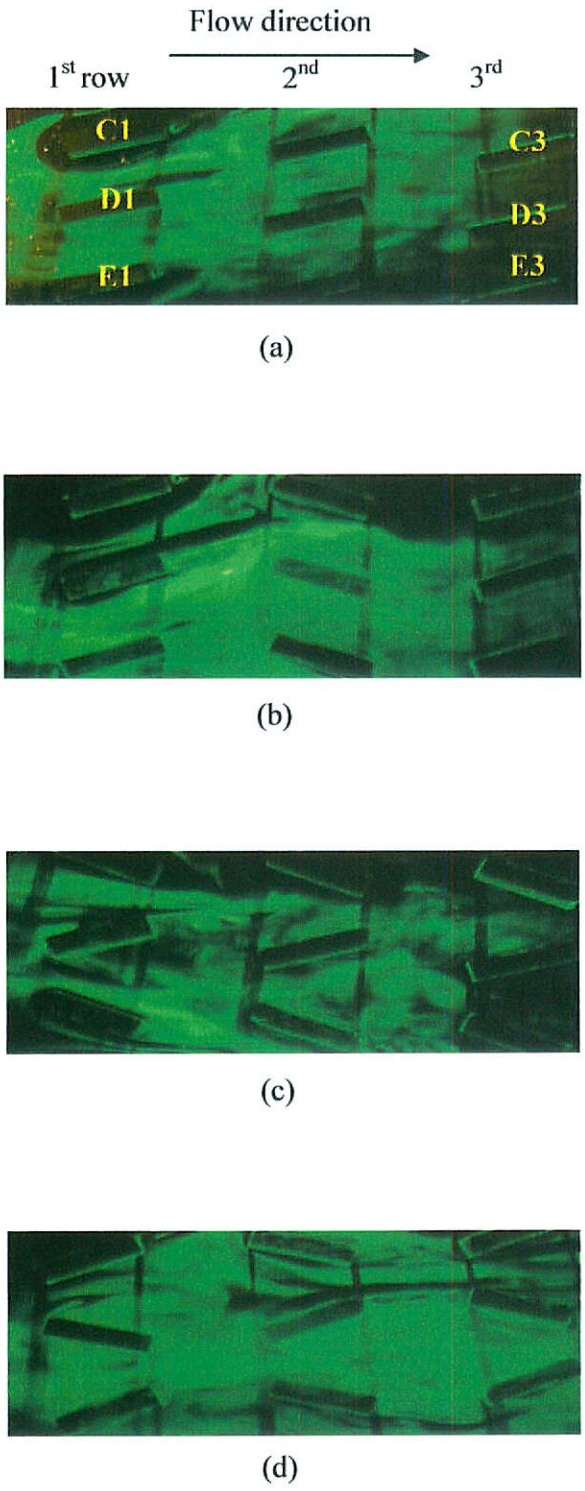

Fig.5.2 Smoke flow visualization at the endwall for Re = 5226 with (a) Co-angular, (b) Zigzag, (c) Co-rotating and (d) Co-counter rotating pattern for H_f = 10 mm in the duct flow.

strongly touched the endwall as well as the following fins. Horseshoe vortexes are still observed.

In co-counter rotating pattern more complicated flow behavior is observed as the consecutive fin rows are opposite in arrangements. In Fig. 5.2(b) and (c) the difference of flow behavior is observed in the middle portion of the consecutive fin rows in streamwise direction. Vortex formed by the diverging pair of the first row fins combined and touched the endwall but this flow is disturbed by the converging pair of the following fins and so heat transfer at that area of the endwall is decreased to some extent.

5.3 Friction factor

To estimate a pressure drop as well as thermal performance with insertion of fins the friction factor for four different fin patterns arranged with three different pitch ratios were measured, and its result were shown in Fig. 5.3. Friction factor, f is obtained from Eq. (3.1). The f values for all the patterns are larger compared with the skin friction on a smooth duct (without fins) which is expressed in the form of Eq. (5.1) for a fully developed turbulent flow.

$$f_s = 0.3164\,\mathrm{Re}^{-1/4} \qquad (5.1)$$

Among the three different values of pitch ratio the largest friction factor is obtained for $PR = 2$ and the lowest value is obtained for $PR = 3.5$. This is because high fin density causes larger restriction to air flow than that of low fin density. On the other hand among the four fin patterns, co-rotating pattern shows the largest friction factor while the co-angular pattern shows the lowest value. This is due to the fact that longitudinal vortex generated by the leading fin row strike the endwall strongly and as the consecutive fin rows are of same co-rotating type every fin rows strike the endwall as well as fin surface strongly. As a result combined larger drag force is occurred. But for co-angular case flow can escape easily through the side just touching the fin and the endwall at the beginning rows due to its co-angular type orientation.

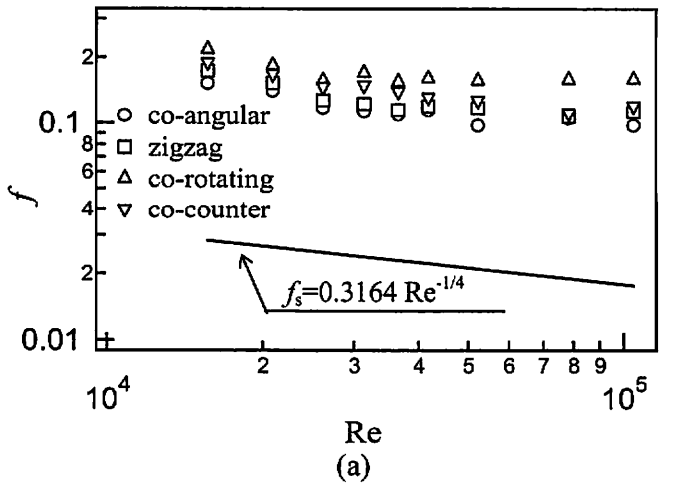

(a)

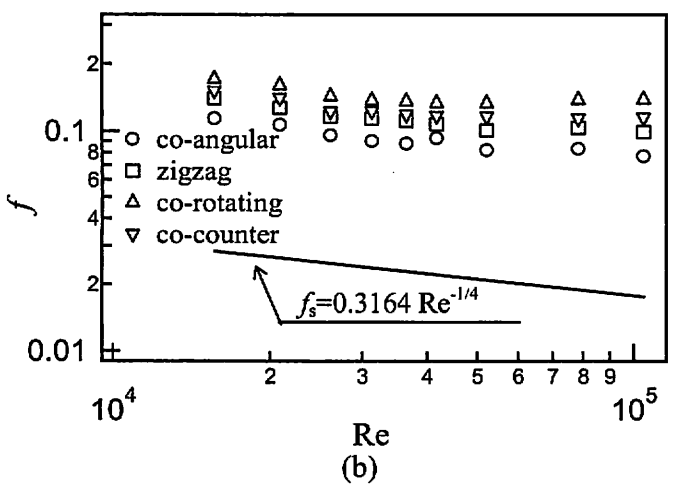

(b)

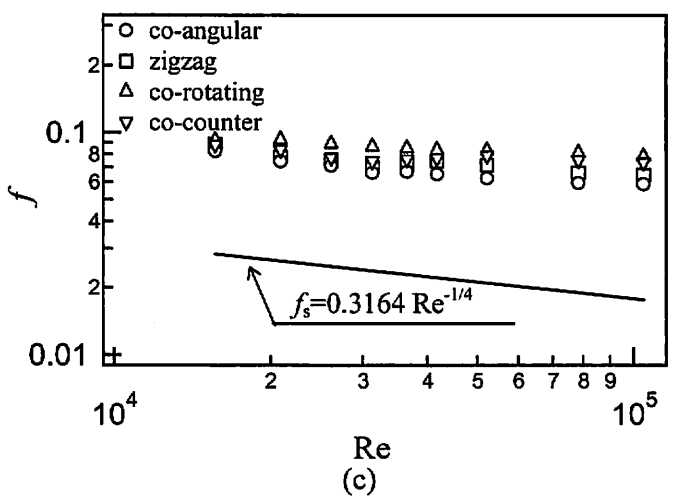

(c)

Fig. 5.3 Variation of friction factor with fin pitch ratio and Reynolds number in a duct with H_f = 10 mm for (a) PR = 2, (b) PR = 3 and (c) PR = 3.5.

Hence the smaller drag force is occurred.

In co-counter rotating case combined longitudinal vortex effect is declined as the consecutive fin rows are opposite in arrangements and hence comparatively lower friction factor is appeared than the co-rotating pattern. As the consecutive fin rows are alternated in directions, zigzag pattern has more contact with the fin surface and consequently a large drag force occurs than for the co-angular pattern. For all fin patterns, f decreases with increase in Reynolds number and pitch ratio, PR.

5.4 Detailed heat transfer analysis

Detailed heat transfer coefficient distributions at the endwall surfaces and the fin base are observed for rectangular fins of all patterns, co-angular, zigzag, co-rotating and co-counter rotating with PR = 2, 3 and 3.5. As for typical examples detailed heat transfer distributions around the representative fin rows of all the patterns for PR = 2 are shown in Figures. 5.4– 5.9. From the infrared images of Fig. 5.4(a), 5.5(a), 5.6(a) and 5.7(a) distinct heat transfer characteristics are observed for co-angular, zigzag, co-rotating and co-counter rotating pattern respectively.

For co-angular pattern as shown in Fig. 5.4(a), the infrared image shows higher heat transfer region are at the fin base and around the fins. This is because flow touches the fin surfaces strongly and so extended surface effect becomes higher. At the same time horseshoe vortexes formed at the front of the fins caused the heat transfer enhancement in that region. Longitudinal vortexes generated by the inclined rectangular fins touches the inter fin region and thereby enhances heat transfer. Behind the fins higher heat transfer regions are also appeared as the corner edges creates more turbulence. Lower heat transfer regions are observed between 3rd row and 4th row fins, i.e., between C3 and C4 fin, D3 and D4 as well as E3 and E4 fin. Profile of these lower heat transfer regions are look like hysteresis curve shaped as already explained in

chapter 3. The same phenomenon is also observed among the successive fin rows i.e. between C4-C5, D4-D5, E4-E5 and the following fins.

In case of zigzag pattern as shown in Fig 5.5(a), heat transfer characteristics similar to co-angular pattern at third fin rows was observed whereas different heat transfer characteristics was appeared at other fin rows as the fins are alternately angled in directions to air flow. Comparatively higher heat transfer regions at the endwall are enlarged in this case than for co-angular pattern. Because the flow touches the endwall and alternated large fin surfaces strongly while the corner effects are still observed. Here, nearly delta shaped lower heat transfer regions are appeared and are different in characteristics than that of co-angular case.

The infrared image of co-rotating pattern, Fig 5.6(a) shows a completely different heat transfer characteristics than for previous two cases. Heat transfer coefficients shows the highest values among the three cases and therefore to visualize the higher and lower heat transfer regions more clearly, heat transfer field was ranged between 100 – 240 W/m^2 K. Here converging and diverging fin pairs form different heat transfer and flow fields. Longitudinal vortexes are generated by each of diverging fin pair, combined and then struck the endwall in inter fin region and front of the following fin pairs which caused heat transfer enhancement from the endwall as well as fin surfaces. Comparatively lower heat transfer regions are observed in front of the diverging fin pairs as diverging fin pairs could not generate such kind of vortex and combined struck to the endwall. Fig. 5.7(a) shows somewhat complicated heat transfer characteristics for co-counter rotating pattern. As the consecutive fin rows are opposite type, longitudinal vortex generated by diverging fin pairs are somewhat disturbed by the following fin pairs and so comparatively lower heat transfer regions are observed in inter fin region. Heat transfer characteristics at every fin rows look different in appearance wherein other fin patterns have their identical appearance at each fin rows.

Now consider Fig. 5.4(b), Fig. 5.5(b), 5.6(b) and 5.7(b) which describe heat transfer

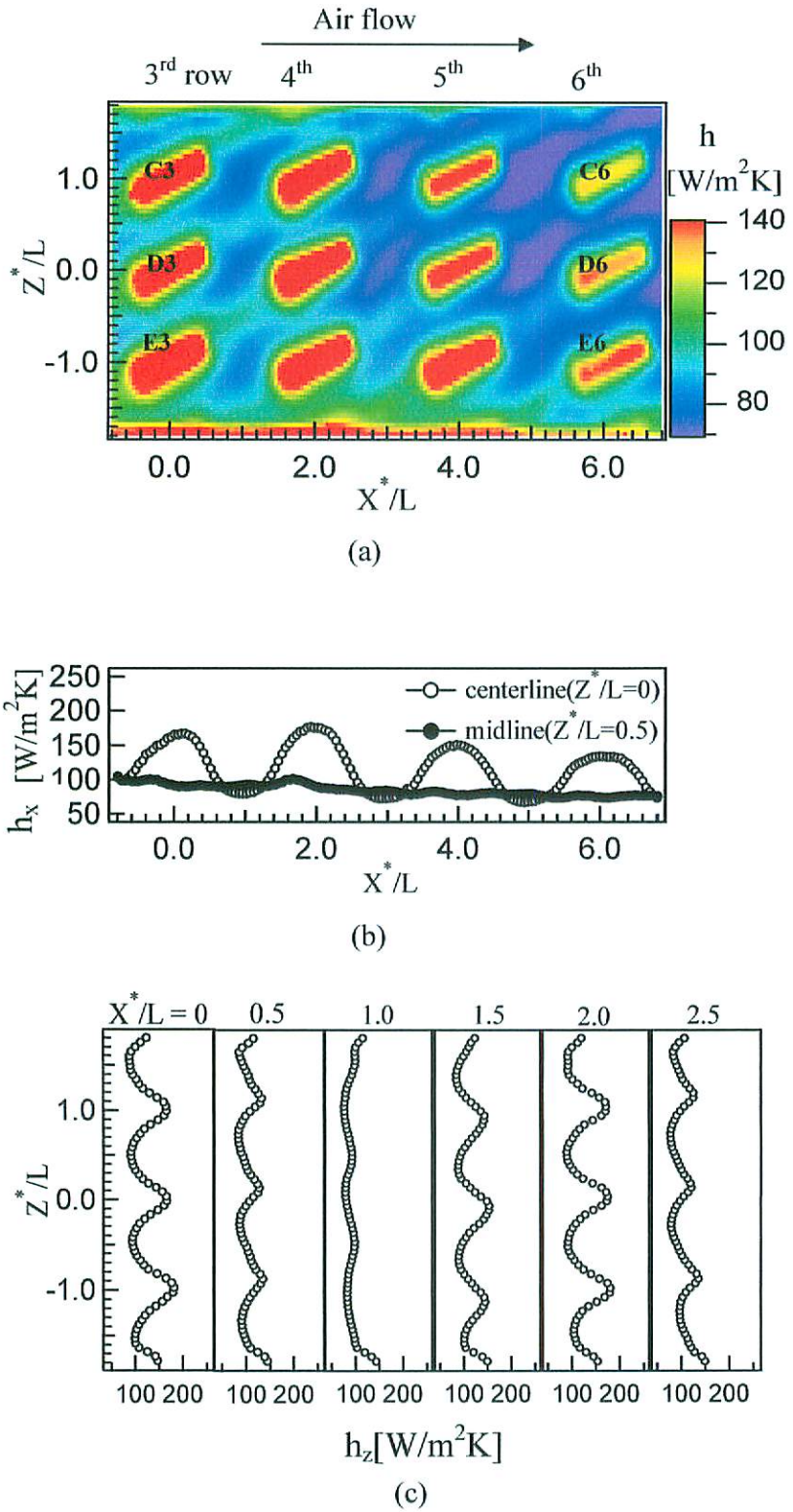

Fig. 5.4 Detailed heat transfer coefficient distributions around the representative fins of co-angular pattern for $Re = 5.22 \times 10^4$, $H_f = 10$ mm and $PR = 2$. (a) Infrared image. (b) Centerline and midline distribution and (c) Spanwise distribution.

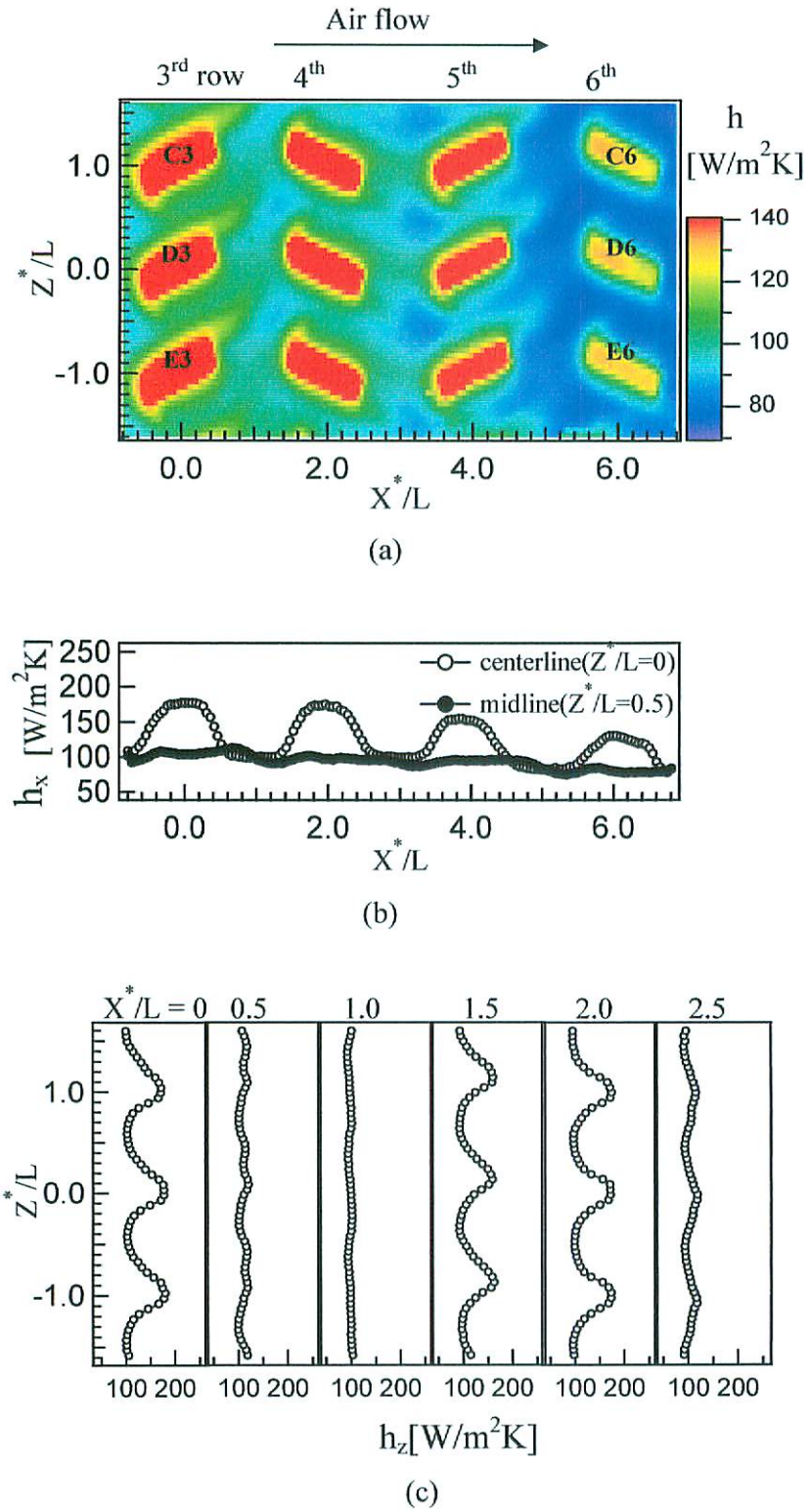

Fig.5.5 Detailed heat transfer coefficient distributions around the representative fins of zigzag pattern for $Re = 5.22 \times 10^4$, $H_f = 10$ mm and $PR = 2$. (a) Infrared image. (b) Centerline and midline distribution and (c) Spanwise distribution.

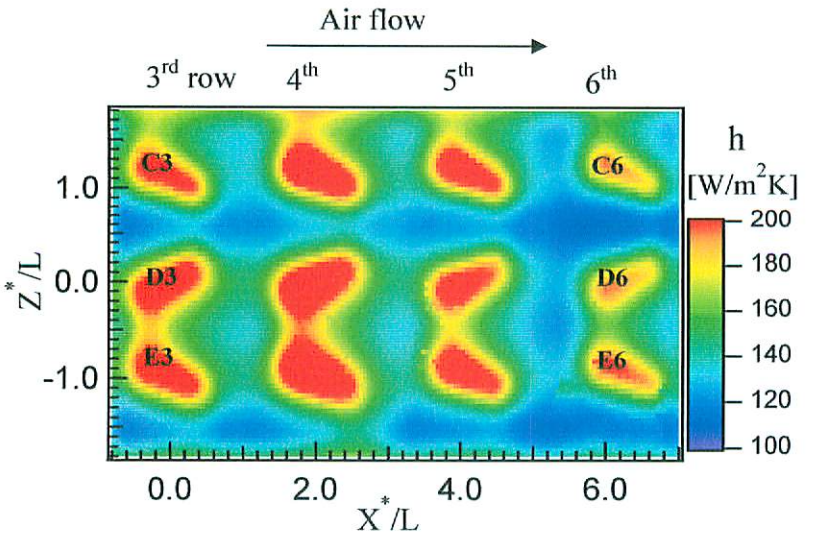

(a)

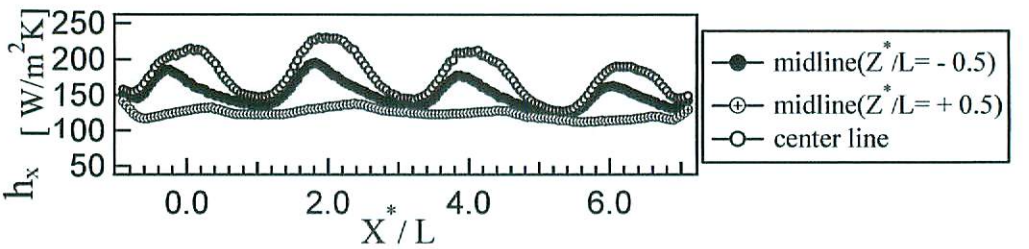

(b)

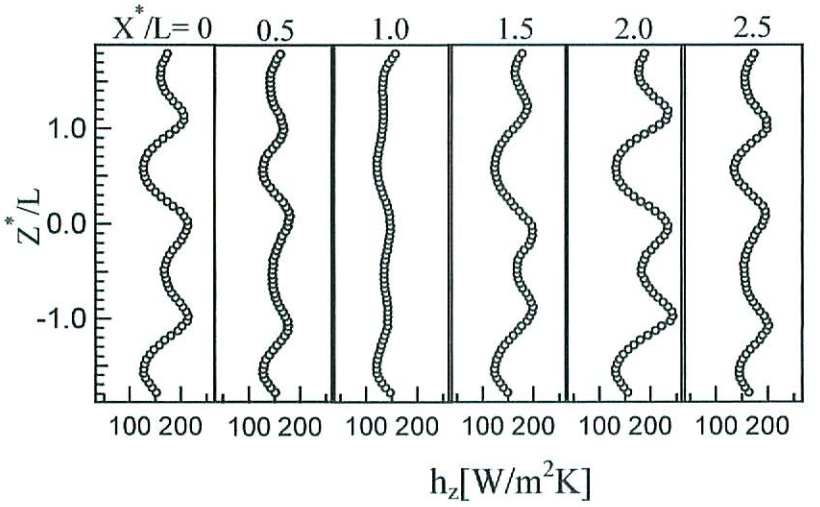

(c)

Fig. 5.6 Detailed heat transfer coefficient distributions around the representative fins of co-rotating pattern for $Re = 5.22 \times 10^4$, $H_f = 10$ mm and $PR = 2$. (a) Infrared image. (b) Centerline and midline distribution and (c) Spanwise distribution.

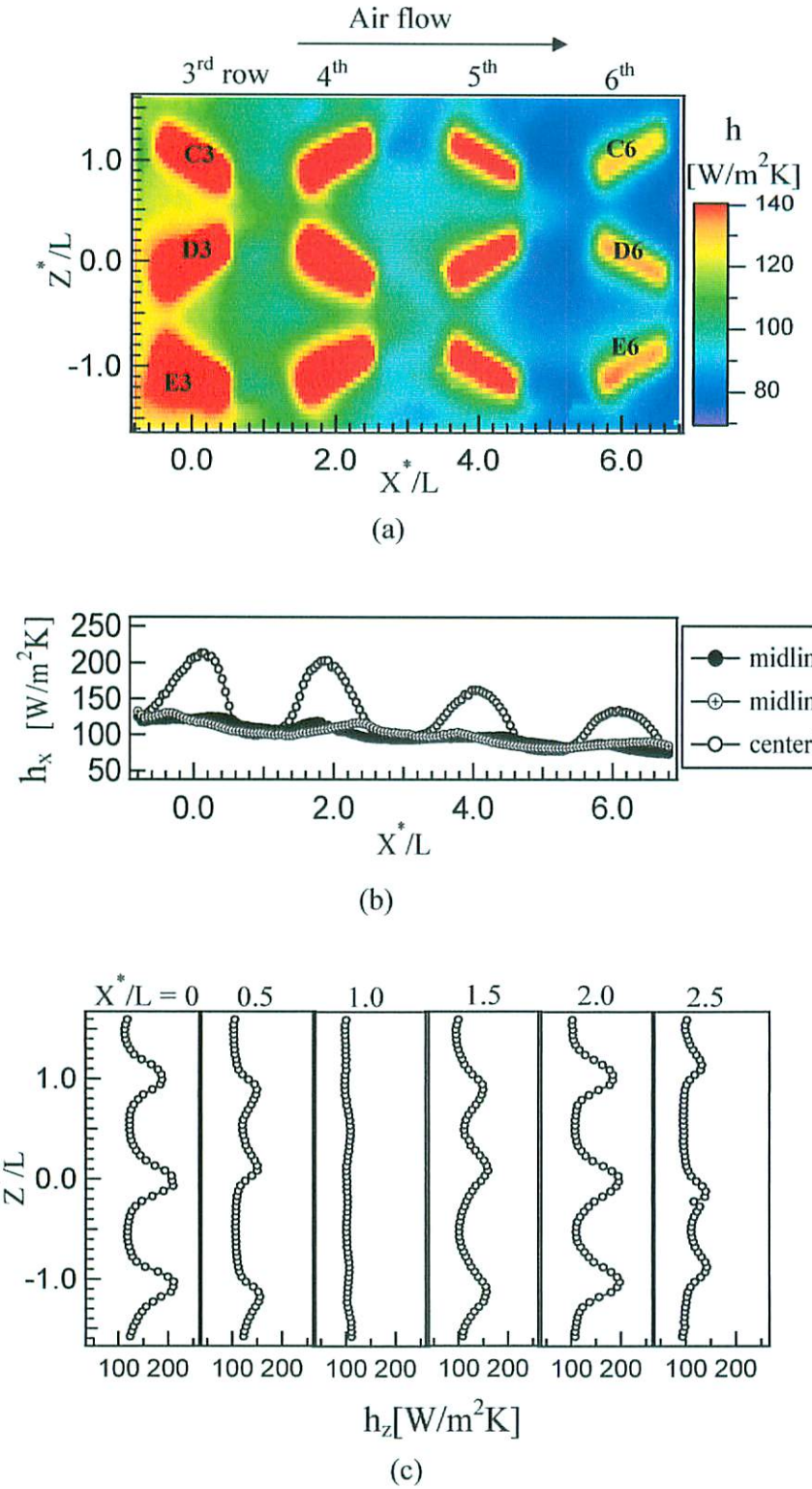

Fig. 5.7 Detailed heat transfer coefficient distributions around the representative fins of co-counter rotating pattern for $Re = 5.22 \times 10^4$, $H_f = 10$ mm and $PR = 2$. (a) Infrared image. (b) Centerline and midline distribution and (c) Spanwise distribution.

coefficient distributions along the center line and midline for co-angular, zigzag, co-rotating and co-counter rotating pattern, respectively. For all patterns periodic distribution is appeared along the center line, showing the local maxima at the fin center and minima at the endwall among fin rows. The maximum and minimum values of local heat transfer coefficient around third and fourth row fins are relatively high, following a subsequent decline along downstream side fins. It is remarkable that centerline distribution in co-rotating pattern possesses the highest local heat transfer coefficient among the four patterns. Midline distribution curve around maxima are flat for zigzag and co-rotating pattern as shown in Fig. 5.5(b) and Fig. 5.6(b) wherein for co-angular and co-counter rotating pattern, curve looks sharp. The midline distribution showing the endwall heat transfer looks nearly flat and half of maximum value for all patterns except for co-rotating pattern. In co-rotating and co-counter rotating case two midline distributions are drawn in order to clarify different flow fields. In co-rotating case midline distribution along Z^*/L= - 0.5 is wavy in nature and local maxima exist just at front of the fin pairs which is different than other cases. Midline distributions for co-rotating pattern achieve the highest heat transfer coefficient among all fin patterns. It might be due to the combined vortex effect formed by diverging fin pairs. Midline distribution along Z^*/L= + 0.5, looks flat and comparatively lower heat transfer coefficients are observed. Just behind the fin pairs heat transfer coefficient values are increased at some extent due to the flow acceleration effect and this behavior continues at every fin rows. In case of co-counter rotating pattern midline distribution along Z^*/L= - 0.5 and + 0.5 looks similar in nature with no significant difference in magnitude between them.

In order to clarify more details of heat transfer characteristics, spanwise heat transfer coefficient distributions at X^*/L = 0, 0.5, 1.0, 1.5, 2.0 and 2.5 are drawn for all patterns as shown in Fig. 5.4(c), 5.5(c), 5.6(c) and 5.7(c). For co-angular pattern (Fig. 5.4(c)) periodical distribution is appeared at X^*/L = 0 and 2.0, i.e. along fin center, while just behind the fins at X^*/L = 0.5 and 2.5 periodical distribution is appeared again though the values of local heat transfer coefficient

are lower than that of fin center. Along the middle between fin rows, i.e. at X^*/L = 1.0, distribution tends toward being flat and the variations of heat transfer coefficient are of lower value. Front of the fins, i.e. at X^*/L = 1.5, heat transfer coefficient distribution turned to periodic.

For zigzag pattern(5.5(c)) at X^*/L = 0 and 2.0 though the trends of heat transfer coefficient distributions is similar to co-angular pattern but the curves around peaks are less sharp than for co-angular pattern, indicating higher heat transfer coefficient at larger area. Just behind the fins at X^*/L = 0.5 and 2.5 the nature of the heat transfer coefficient distribution are different than that of co-angular pattern.

In case of co-rotating pattern (5.6(c)), at X^*/L =0 and 2.0 identical heat transfer distributions are appeared along fin center of third and fourth rows. In this case, in the middle of converging fin pairs and in the middle of diverging fin pairs heat transfer profile are different, comparatively lower heat transfer coefficient values are appeared in the middle position between converging fin pairs than that of diverging fin pairs though heat transfer coefficient at fin center remains same at every fin. Just behind the fins, i.e. at X^*/L = 0.5 and 2.5 curves are found to be straightened. Along the middle between fin rows at X^*/L = 1.0, distributions looks flat while at front of the fin distributions tend to periodic.

In case of co-counter rotating pattern (5.7(c)), identical heat transfer distributions are appeared along fin center i.e. at X^*/L = 0 and 2.0. At X^*/L = 0.5, distribution in the middle of diverging fin pairs as well as converging fin pairs are identical to the following diverging and converging fin pairs respectively at X^*/L =2.5. At the middle of the third and fourth rows distribution is almost flat. Considering the spanwise distributions, it is recognized that co-rotating pattern experiences the highest heat transfer among four types of fin pattern because of combined vortex effect and larger flow interactions.

5.5 Area-averaged heat transfer coefficient

The area-averaged heat transfer coefficients at the endwall and for the overall surfaces of the representative third, fourth and fifth row fins were measured from infrared images with the Eq.(4.3). And then we calculated average Nusselt number based on hydraulic diameter of the duct and average heat transfer coefficient. Since Nusselt number is based on the average heat transfer coefficient of the projected surface area, it will reflect the effect of variation on the surface area, fin pattern as well as that of flow behavior formed by different fin pattern. Fig.5.8 show the characteristics of the area averaged Nusselt number for overall surface area with Reynolds number for different fin pattern with PR = 2, 3 and 3.5. The area averaged Nusselt number is further represented by the curve fitted lines. All the data fall smoothly on the curve fitted lines and can be well represented as the form of Eq. (4.4). Values of c for different fin pattern and PR are listed in Table 2.

From Fig.5.8 (a), (b) and (c), we got that the Nusselt number has a maximum value for the co-rotating case among different fin patterns and is independent of PR. On the other hand Nusselt number has the minimum value for co-angular pattern. This higher heat transfer for co-rotating pattern is already explained as due to the combined vortex effect of diverging fin pairs. From the Table 2 and Fig.5.8, it is observed that maximum heat transfer occurred at PR = 2 and in general heat transfer decreases with increasing PR except for co-counter rotating pattern. It is

Table 2 Coefficient of heat transfer correlations for different fin pattern, pitch ratio and fin height of 10 mm at a narrow duct of 50 mm height

Pattern	$\overline{Nu}_{overall} = c\,Re^{0.7}$		
	c		
	PR = 2	PR = 3	PR = 3.5
Co-angular	0.163	0.153	0.149
Zigzag	0.175	0.176	0.168
Co-rotating	0.261	0.223	0.212
Co-counter	0.191	0.169	0.191

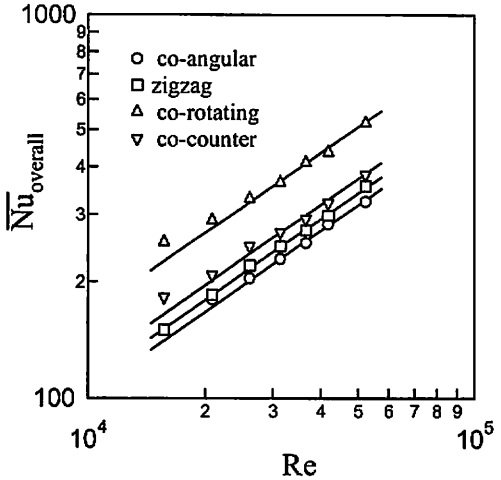

(a) $PR = 2$

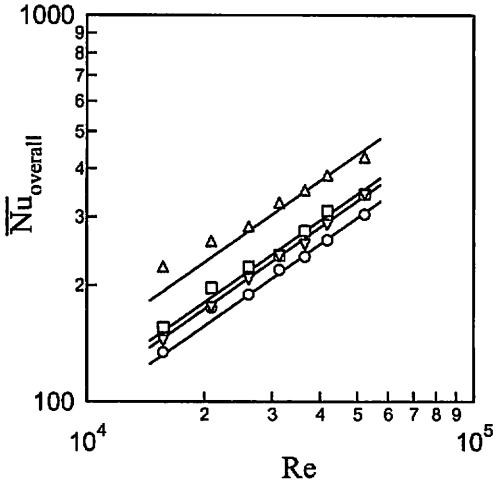

(b) $PR = 3$

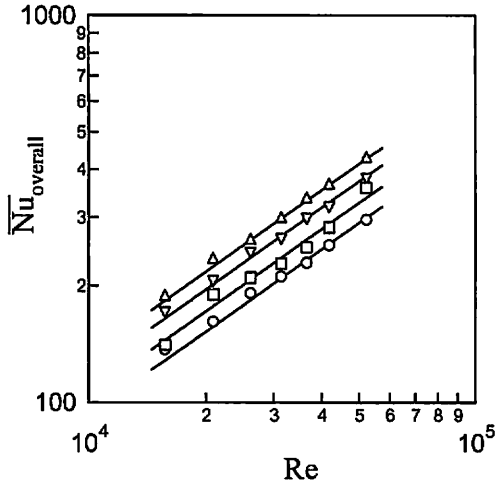

(c) $PR = 3.5$

Fig. 5.8 Area- averaged Nusselt numbers at the overall surface with different fin patterns for (a) $PR = 2$, (b) $PR = 3$ and (c) $PR = 3.5$

also found in Fig. 5.8(b) that at $PR = 3$, zigzag pattern pronounces slightly higher heat transfer than for co-counter rotating pattern which shows difference than for $PR = 2$ and 3.5. The difference of heat transfer enhancement among four fin pattern is found evenly spaced which is dissimilar than that of $PR = 2$ and 3 as shown in Fig. 5.8(c).

The characteristics of area averaged Nusselt number of overall surface with Reynolds number at different PR for only co-rotating pattern is shown in Fig. 5.9. Plots are then curve fitted and can be represented by the Eq.(4.4). Values of c are listed in Table 3 and it is shown that co-rotating pattern experiences a maximum overall heat transfer enhancement for $PR = 2$. The difference of heat transfer enhancement for $PR = 3$ and 3.5 is little compared to $PR = 2$ and others.

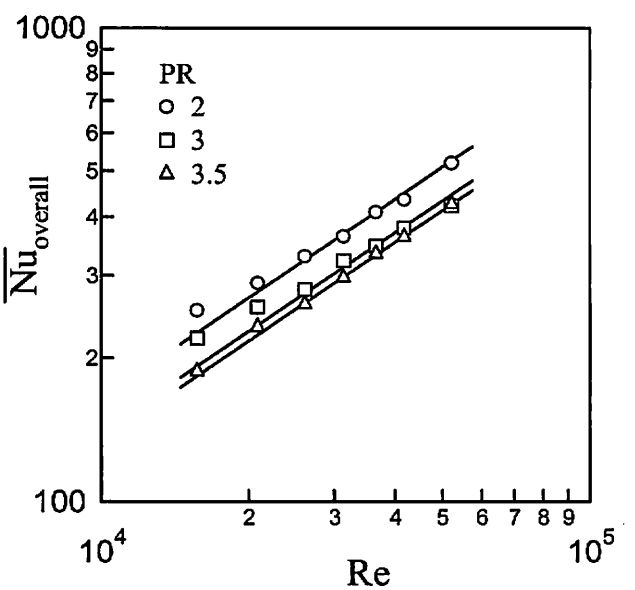

Fig. 5.9 Area-averaged Nusselt numbers at the overall surface for co-rotating pattern with different fin pitch ratio.

Table 3 Coefficients of heat transfer correlations for different PR of co-rotating pattern at a duct of 50 mm height.

Pitch ratio, PR	$\overline{Nu}_{overall} = c\,Re^{0.7}$
	c
2	0.261
3	0.223
3.5	0.212

In order to know the effect of extended surface or vortex on heat transfer enhancement, especially for the co-rotating pattern, the most effective fin arrangement, the variation of area averaged Nusselt number at the overall surface area and fin base with Reynolds number for different fin height are drawn as shown in Fig. 5.10(a) and (b). Plots are curve fitted and well

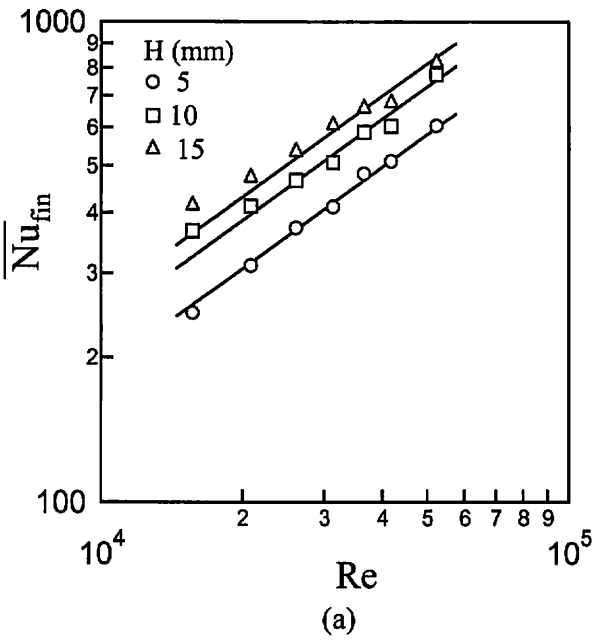

(a)

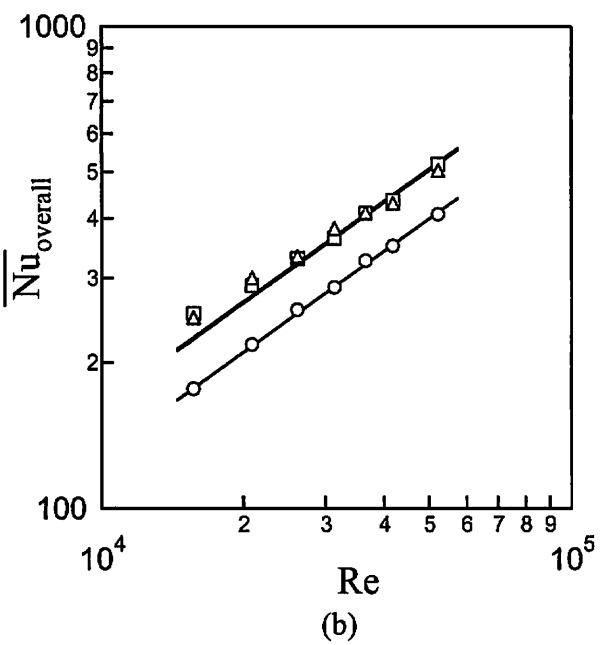

(b)

Fig. 5.10 Variation of area–averaged Nusselt number for the co-rotating pattern at the (a) overall surface and (b) fin base with different fin height

represented by the Eq.(4.4). Values of c are listed in Table 4. From Fig. 5.10 and Table 4, we found that 10 mm fin causes the maximum heat transfer though the difference of overall heat transfer enhancement is very little between 10 and 15 mm height fin which was also observed previously for co-angular pattern [2007]. On the other hand in case of heat transfer through the fin base only, 15 mm fin has the maximum heat transfer while 5 mm fin has the lowest heat transfer which indicates actually the extended surface effect. So it is recognizable that 10 mm fin causes more turbulence and vortex effect than 15 mm fin, as a result overall heat transfer, i.e. extended surface effect and vortex effect on fin and endwall for 10 mm fin has the highest value. At the same time, pressure drop for 10 mm fin might be lower than for 15 mm fin, so it is suitable to choose 10 mm fin for the higher thermal performance.

Table 4
Coefficients of heat transfer correlations for fin base and overall surface with different fin height of co-rotating pattern at a duct height of 50 mm.

Height, H (mm)	$\overline{Nu} = c\,\mathrm{Re}^{0.7}$	
	c	
	Fin base	Overall surface
5	0.298	0.205
10	0.375	0.261
15	0.419	0.259

5.6 Thermal performance ratio

Various techniques may be proposed for evaluating the thermal performance ratio according to the purpose for which a heat exchanger is designed [1974]. Here the heat transfer enhancement rate will be evaluated for the promoter case keeping the pumping power and heat transfer area constant. In this case the relation between Re and Re_s at the smooth surface can be derived from the limiting condition and written as the following equation [1972].

$$Re_s = Re(f/f_s)^{\frac{1}{3}} \tag{5.2}$$

Where, f_s is the friction factor at the smooth surface. Substituting $f_s = 0.3164Re_s^{-1/4}$ into the Eq.(5.2) yields the following Eq. 5.3.

$$Re_s = (fRe^3/0.3164)^{1/2.75} \tag{5.3}$$

Corresponding Nusselt number of smooth duct is then calculated by

$$Nu_s = 0.019\,\mathrm{Re}_s^{0.8} \tag{5.4}$$

Finding Nu_s for Re_s, we have the heat transfer augmentation rate and the ratio of heat transfer coefficient of present system to smooth duct is defined as thermal performance accounting pressure drop under the pumping power and heating surface to be kept constant.

$$\eta = \overline{h_x}/h_s = \overline{Nu}/Nu_s \tag{5.5}$$

The indication from the Eq. (5.5) is that there will be a net energy gain only if η is greater than unity. Fig. 5.11 shows the relation between η (thermal performance ratio) and $f^{1/3}$ Re for different fin patterns. It is seen from this figure that η slowly decreases with increasing Re for all cases and it varies between 1.8 –3.25 indicating the substantial heat transfer augmentation for all cases. Among the four kinds of fin patterns co-rotating patterns appears to be one of the most attractive configuration since it produces the highest overall heat transfer enhancement with slightly higher pressure penalty due to the pronounced vortex effect on both the endwall and fin surfaces. It is

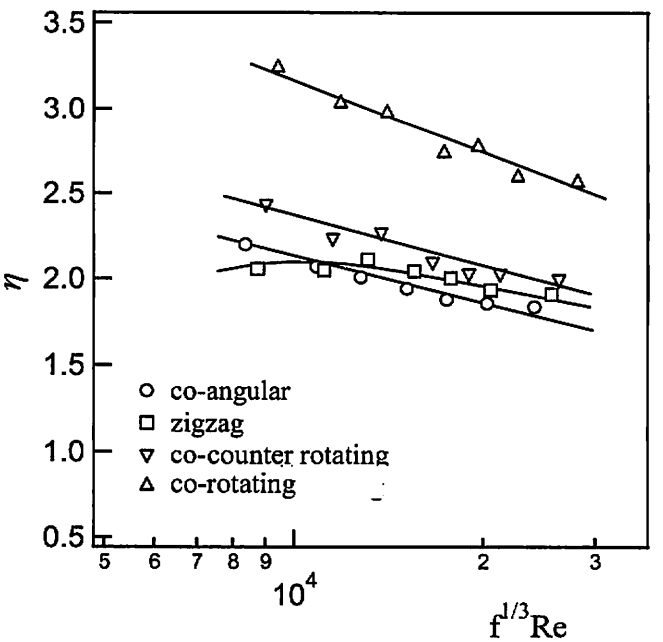

Fig. 5.11 Relation between η and $f^{1/3}Re$

also notable that the difference of thermal performance ratio η among the co-angular, zigzag and co-counter rotating is smaller where as a big difference is appeared between co-rotating and other cases. However a substantial enhancement is achieved in the order of co-rotating, co-counter rotating, zigzag and co-angular pattern while the same order was shown for the friction factor. The feature of the zigzag pattern shows a different characteristic than the other cases. Initially thermal performance increases with Reynolds number and then decreases with increasing the Reynolds number. This might be due to the larger friction forces at the lower Reynolds number.

5.7 Summary

After performing the experimental investigation we can summarize the major contribution as follows:

First we provided detailed heat transfer distributions on the overall surface for four different fin patterns and then we calculated the area averaged heat transfer coefficient and differentiated the effect of extended surface and endwall surface on heat transfer enhancement. Oil titanium oxide flow pattern and smoke flow visualization simplified the heat transfer mechanism. Finally thermal performance ratio was evaluated and find thereby:

1. The friction factors for all fin patterns are larger compared to the skin friction on the smooth surface for a fully developed turbulent flow. Among the four patterns largest friction factor was developed for the co-rotating pattern owing to the strong flow interactions and combined vortex attack on the endwall and fin surface whereas the least friction developed for co-angular pattern.

Friction factor value is slowly decreased with increasing Reynolds number and pitch ratio, *PR*.

2. Smoke flow pattern around the fins and oil titanium oxide film flow pattern on the endwall shows a good agreement with each other. Horseshoe vortex is shown apparently dominant in case of co-angular fin pattern whereas in case of zigzag fin pattern wavy flow behavior was observed. In case of co-rotating fin pattern more tortuous flow is observed as the longitudinal vortexes generated by diverging fin pairs combinedly attack the endwall and fin surfaces. This flow was somewhat disturbed by the following converging fin pairs in case of co-counter rotating fin pattern.

3. The effect of fin height on area averaged Nusselt number ($\overline{Nu}_{overall}$) for smallest *PR* and co-rotating pattern it is found that 10 mm fin has the maximum value and the difference of

Nusselt number between 10 mm and 15 mm fin is very little. The same effect was also observed in case of co-angular pattern [2007].

4. The area averaged Nusselt number on overall surface area ($\overline{Nu}_{overall}$) increases with increasing the Reynolds number regardless of fin patterns and pitch ratio (*PR*). Co-rotating pattern has the highest Nusselt number and the co-angular pattern has the least Nusselt number. Considering the pitch ratio, $PR = 2$ shows the highest Nusselt value and the value is decreased with increasing *PR* for all fin patterns.

5. When the thermal performance is considered, among the four kinds of fin patterns co-rotating pattern with $PR = 2$ and $H_f = 10$ mm is the most recommended configuration since it produces the highest overall heat transfer enhancement with slightly higher pressure penalty due to the pronounced vortex effect on both the endwall and fin surfaces. Heat transfer enhancement with co-rotating pattern is more than three times the fin-less duct. Contrarily, co-angular pattern is the least recommended.